Journal of
Polymer & Composites

ISSN: 2321-2810 (Online)
ISSN: 2321-8525 (Print)
Volume 14, Special Issue 2, 2026
DOI (Journal): 10.37591/JoPC

https://journals.stmjournals.com/jopc

Research JoPC

Thermo–Electrical Performance Enhancement of a Lightweight Polymer–Metal Hybrid Electrostatic Precipitator Using Epoxy-Based Composite Housing for Industrial Particulate Control

Bharat Mankar[1], Yash Gopale[1], Sakshi Balghare[1], Prasad Jadhav[1], Pramod Kothmire[2]*

Abstract

Airborne particulate emissions, particularly PM_{10} and $PM_{2.5}$ produced by industrial activities and combustion processes, they continue to pose a significant threat to both the environment and public health. Electrostatic precipitators (ESPs) are widely recognized for their ability to achieve high collection efficiencies; however, conventional metallic constructions often lead to increased system weight, higher fabrication costs, and long-term corrosion-related challenges. In this study, a lightweight hybrid material approach is proposed by integrating an epoxy-based polymer composite (glass fiber–reinforced epoxy, GFRE) as the external housing material, combined with stainless steel discharge and collecting electrodes. The epoxy-based composite is selected due to its low density, high corrosion resistance, electrical insulation capability, and ease of fabrication, making it an attractive alternative to traditional metallic casings such as aluminium. Stainless steel electrodes are retained for their superior electrical conductivity, mechanical strength, and stability under high-voltage corona discharge conditions (18–22 kV). This hybrid material configuration enables improved structural efficiency while maintaining reliable electrostatic performance. A coupled thermo-electrical and fluid flow analysis is performed using computational fluid dynamics (CFD) and analytical modeling to evaluate the influence of material selection on ESP performance. Key parameters such as electric field distribution, particle migration velocity, pressure drop, and thermal behavior are systematically analyzed. The results indicate that the incorporation of the epoxy-based composite significantly reduces the overall system weight while maintaining uniform electric field distribution and stable corona generation. Additionally, the polymer housing minimizes thermal losses and enhances corrosion resistance, thereby improving long-term durability. The study highlights that polymer–metal hybrid ESP designs offer a promising pathway toward lightweight, energy-efficient, and cost-effective air pollution control systems, aligning with the growing demand for sustainable industrial technologies.

Keywords: Electrostatic precipitator, epoxy composite, polymer–metal hybrid system, $PM_{2.5}$ removal, thermo-electrical performance, lightweight design, CFD analysis

***Author for Correspondence**
Pramod Kothmire
ppkothmire@mitaoe.ac.in

[1]UG Scholar, Department of Mechanical Engineering, MIT Academy of Engineering, Alandi, Pune, Maharashtra, India
[2]Associate Professor, Department of Mechanical Engineering, MIT Academy of Engineering, Alandi, Pune, Maharashtra, India

Received Date: April 15, 2026
Accepted Date: April 22, 2026
Published Date: May 02, 2026

Citation: Bharat Mankar, Yash Gopale, Sakshi Balghare, Prasad Jadhav, Pramod Kothmire. Thermo–Electrical Performance Enhancement of a Lightweight Polymer–Metal Hybrid Electrostatic Precipitator Using Epoxy-Based Composite Housing for Industrial Particulate Control. Journal of Polymer & Composites. 2026; 14(Special Issue 2): S652–S668p.

INTRODUCTION

Electrostatic precipitators (ESPs) have emerged as one of the most reliable and energy-efficient technologies for controlling particulate emissions from industrial exhaust streams. By utilizing electrostatic forces, ESPs effectively remove fine particles such as PM_{10} and $PM_{2.5}$ without imposing significant pressure losses on the system. In a typical configuration, suspended particles are electrically charged through corona discharge and subsequently driven toward oppositely charged collecting plates, where they are deposited and removed. Conventional ESP systems generally employ vertically aligned metallic plates—commonly mild steel or stainless steel—with inter-plate spacing in the range of 15–30 cm, ensuring adequate electric field distribution and gas flow passage [1, 2]. The widespread adoption of ESPs across industries such as cement manufacturing, thermal power plants, waste incineration, and air purification systems is primarily attributed to their high collection efficiency, often exceeding 99%, and their capability to handle large volumetric flow rates. However, with increasing emphasis on sustainability, energy efficiency, and material optimization, there is a growing need to rethink traditional ESP designs, particularly in terms of material selection and structural configuration.

Material properties play a crucial role in determining ESP performance, as they directly influence corona stability, electrical conductivity, thermal behavior, and resistance to corrosion and erosion. While aluminium has been widely used for casings due to its lightweight nature and good thermal conductivity, and stainless steel remains the preferred choice for electrodes due to its durability and electrical stability, recent advances in material science have introduced polymer-based composites as promising alternatives. In this context, epoxy-based polymer composites, particularly glass fiber–reinforced epoxy (GFRE), offer significant advantages such as low density, excellent corrosion resistance, electrical insulation, and ease of fabrication. These properties make them highly suitable for ESP housing and structural components, especially in environments where chemical exposure and thermal fluctuations are critical. The integration of such lightweight polymer materials with metallic electrodes presents a hybrid design approach, enabling improved structural efficiency, reduced system weight, and enhanced durability without compromising electrostatic performance.

LITERATURE REVIEW

The performance of electrostatic precipitators is governed by a complex interaction of electrical, fluid dynamic, and material parameters. Classical studies [3, 4] have established that applied voltage, electric field strength, and particle migration velocity are primary factors controlling particle collection efficiency. These parameters are further influenced by particle characteristics such as size distribution, electrical resistivity, and drag forces within the gas stream. In addition to electrical parameters, geometric design aspects—including plate spacing, electrode configuration, and specific collection area (SCA)—have been shown to significantly affect ESP efficiency and pressure drop characteristics [5, 6]. Improper flow distribution and sneakage losses can lead to reduced collection efficiency, highlighting the importance of optimized design.

With the advancement of computational tools, numerical modelling techniques such as the finite volume method (FVM) and finite element method (FEM) have been extensively applied to simulate electrohydrodynamic behavior in ESPs [7–10]. These studies provide detailed insights into electric field distribution, corona discharge characteristics, and particle trajectories under varying operating conditions. Further investigations have incorporated the effects of temperature, humidity, and dust loading, demonstrating their significant influence on particle charging mechanisms and collection efficiency [11–14]. Despite these advancements, several challenges persist, particularly in scaling laboratory findings to industrial applications, understanding transient dust accumulation, and predicting long-term electrode fouling and performance degradation [15–18].

Recent research has increasingly focused on material innovation and polymer integration in ESP systems, particularly within the scope of advanced composite materials. Studies reported [19–23] highlight the use of epoxy-based and fiber-reinforced polymer materials for lightweight structural applications, improved corrosion resistance, and enhanced durability in harsh environments. These works demonstrate that polymer composites can significantly reduce system weight while maintaining structural integrity and thermal stability. Additionally, investigations on electrostatic separation and multi phase flow systems emphasize the importance of coupled electric field–fluid flow interactions in determining separation efficiency and device performance (Kothmire et al., 2020; Kothmire et al., 2023) [24, 25]. CFD-based studies on electrostatic filters and fluid separators further validate the role of integrated modelling approaches in optimizing geometry and improving system efficiency (Shinde et al., 2018; Katkade et al., 2022) [26,27]. For instance, Kumar et al. [28] discussed the growing importance of sustainable fiber materials and highlighted their potential in improving structural and thermal efficiency. Similarly, Zhang et al. [29] examined the role of chemical treatment in modifying bio-based composites, demonstrating notable improvements in thermal stability and mechanical strength. Further, Patel et al. [30] investigated polymer-based composite fibers and reported enhanced durability and performance under varying loading conditions, making them suitable for advanced engineering systems. In addition, Singh et al. [31] explored lignocellulosic fiber composites and emphasized their potential as lightweight and thermally efficient alternatives to conventional materials. Extending this perspective, Demir and Kaya [32] experimentally analyzed heat exchanger performance using alternative materials and concluded that material selection plays a crucial role in improving overall thermal efficiency. Kothmire et al., 2020 [33] presented the effect of frequency on separation of water from water-in-oil emulsion along with the bottom grounding of the electrostatic vessel. Collectively, these studies underline the increasing relevance of polymer and fiber-based materials in thermal system design, particularly in applications such as heat exchangers and energy systems where both performance and sustainability are critical.

RESEARCH GAP AND SCOPE

From the literature, it is evident that while extensive research has been conducted on ESP performance in terms of electrical and flow parameters, limited attention has been given to the integration of lightweight polymer composites in ESP structural design, particularly in hybrid configurations combining polymers with metallic electrodes. The potential benefits of such materials—reduced weight, enhanced corrosion resistance, and improved manufacturability—remain under explored in the context of electrostatic precipitation systems. Furthermore, most existing studies focus either on analytical models or simplified numerical simulations, with relatively few investigations addressing coupled thermo-electrical–fluid interactions in polymer–metal hybrid ESP designs. Therefore, the present study aims to bridge this gap by 1) Developing a polymer–metal hybrid ESP design using epoxy-based composite housing and stainless steel electrodes 2) Evaluating thermo-electrical and flow performance using CFD and analytical modelling 3) Investigating the influence of material properties, operating voltage, and particle characteristics, and 4) Exploring the feasibility of lightweight, corrosion-resistant, and energy-efficient ESP systems aligned with modern industrial and environmental requirements.

This approach contributes to the advancement of next-generation ESP technologies, particularly within the scope of polymer-based engineering applications.

METHODOLOGY

The present investigation adopts a multi-physics modelling framework combining computational fluid dynamics (CFD), electrostatic field analysis, and analytical modelling to evaluate the thermo-electrical performance of a three-stage electrostatic precipitator (ESP) incorporating polymer-assisted lightweight design. The methodology is structured to capture the coupled interaction between fluid flow, electric field distribution, particle dynamics, and material behaviour, thereby ensuring a realistic representation of industrial operating conditions. The proposed methodology introduces several unique contributions 1) Integration of epoxy-based polymer composites in ESP design 2) Coupled electrostatic–CFD modelling with material-specific properties 3) Development of a three-stage hybrid filtration system 4) Simultaneous evaluation of thermal, electrical, and particulate behaviour

MATERIAL SELECTION AND POLYMER INTEGRATION

In addition to conventional metallic components, this study introduces a high-performance epoxy-based polymer composite coating (glass-fiber reinforced epoxy – GFRE) applied over selected internal surfaces and structural supports. The inclusion of this polymer layer serves multiple functions electrical insulation enhancement, stabilizing corona discharge, weight reduction compared to fully metallic casings, improved corrosion resistance under humid and chemically active flue gases, and thermal damping, minimizing localized hot spots. The ESP configuration thus consists of Aluminium outer casing (lightweight, high thermal conductivity), Stainless steel electrodes (robust electrical performance), and Epoxy-based polymer composite layers (insulation and durability enhancement). This hybrid material system enables a balanced thermo-electrical response, aligning with emerging research themes on polymer-integrated engineering systems.

COMPUTATIONAL MODELLING FRAMEWORK

A three-dimensional model of the ESP is developed using ANSYS Fluent, incorporating both electrostatic and fluid domains (Figures 1–4). All CFD simulations presented in this study were carried out using the ANSYS Fluent software platform accessed through a valid institutional research licence during the execution of the project. The modelling approach integrates electrostatic module solves electric potential and field distribution and captures corona discharge behaviour between electrodes. The CFD Module (ANSYS Fluent) simulates airflow, temperature distribution, and particle trajectories. This accounts for turbulence, pressure drop, and residence time. The coupled Multiphysics approach links electric field with particle charging and migration. And it incorporates polymer layer influence on dielectric properties and heat transfer. This integrated approach provides deeper insight into electro-hydrodynamic behaviour, which is often overlooked in simplified ESP analyses.

GEOMETRY AND THREE-STAGE CONFIGURATION

The ESP geometry consists of an inlet duct, expansion chamber, collection region, and outlet diffuser (Figure 4). A three-stage filtration concept is implemented to enhance overall performance. There are three stages, stage 1 consists of mechanical pre- filter which removes coarse particles and protects downstream components. The stage 2 is electrostatic collection zone which is also acts as high-voltage corona which discharge ionizes particles, which are collected on stainless steel plates. The stage 3 is polymer-assisted Carbon filtration which activated carbon supported on polymer substrate removes ultra-fine particles, gases, and odours. The addition of polymer-supported filtration enhances adsorption efficiency and structural flexibility, representing a novel design feature.

MESHING STRATEGY

The computational domain is discretized using an unstructured tetrahedral mesh (Figure 5) to accurately capture complex geometrical features. The key aspects includes local mesh refinement near electrodes and high-gradient regions, optimized element size to balance accuracy and computational cost, and growth rate control (1.2) for smooth mesh transition. The mesh quality ensures reliable prediction of velocity gradients, electric field variations, and particle trajectories (Table 1).

Figure 1. 3D model of a three-stage dust-settling exhaust chamber showing the inlet, dual settling

zones, dust collector, and outlet for slowed airflow, particle settling, and clean air release.

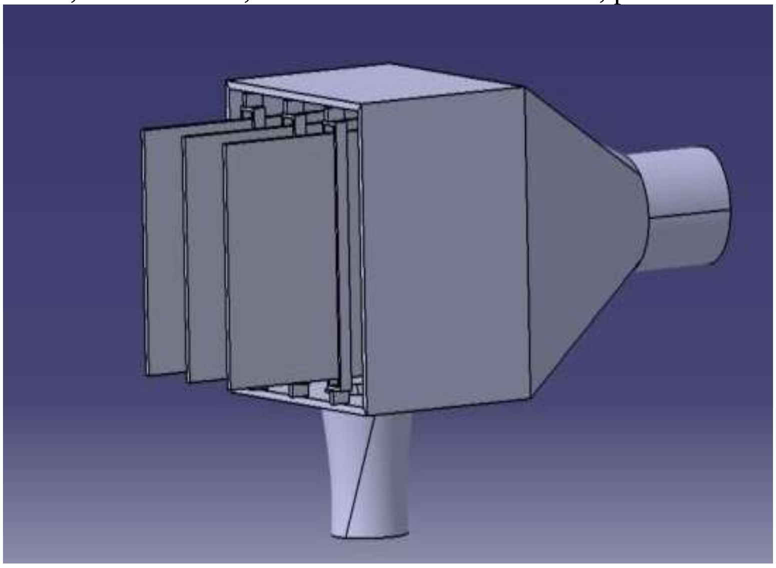

Figure 2. Vertical plate of a three-stage electrostatic precipitator.

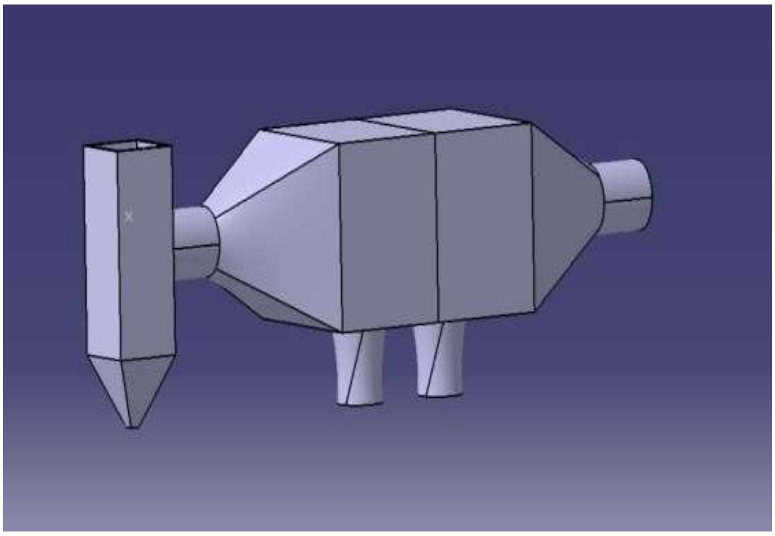

Figure 3. CAD model of a three-stage electro- static precipitator.

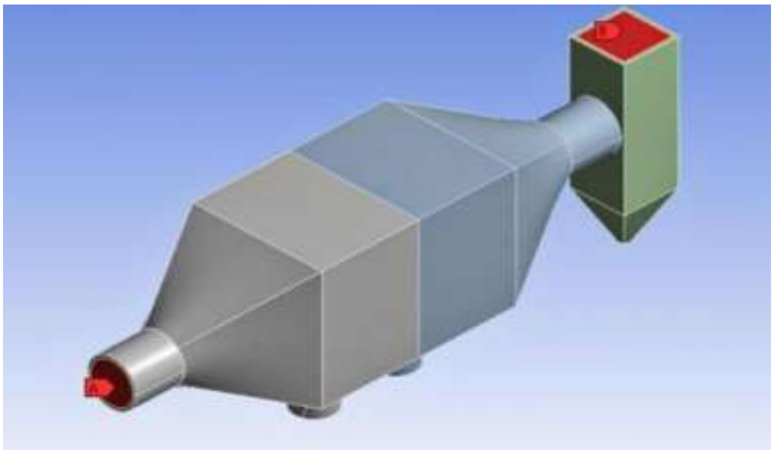

Figure 4. 3D geometry model of a gas filtration chamber with inlet , main chamber, dust collection hopper, and outlet.

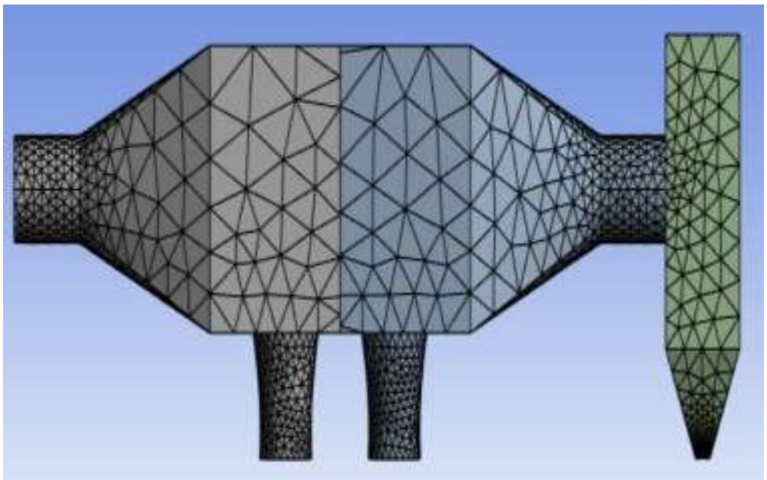

Figure 5. ESP model with unstructured mesh using varied element sizes for accurate airflow.

Table 1. Details of mesh settings.

Property	**Value**
Display style	Use Geometry Setting
Physics preference	CFD
Solver preference	Fluent
Element size	5.0×10^{-3} m
Export format	Standard
Export preview surface mesh	No
Use adaptive sizing	No
Growth rate	Default (1.2)
Max size	Default (0.1 m)
Mesh defeaturing	Yes
Defeature size	Default (2.5×10^{-3} m)
Curvature min size	Default (5.0×10^{-3} m)
Curvature normal angle	Default (18°)
Bounding box diagonal	1.816 m
Average surface area	6.3038×10^{-3} m²
Minimum edge length	3.5714×10^{-5} m

BOUNDARY CONDITIONS AND OPERATING PARAMETERS

Simulations are performed under realistic industrial conditions. The boundary conditions which are used are at Inlet (Gas Flow) the specified velocity and particulate loading was assigned. At outlet, the pressure outlet with zero gauge pressure was assigned. For walls, no-slip condition was assigned. The Electrodes were simulated by assigning high-voltage potential (18–22 kV). Polymer-coated surfaces are modeled with modified dielectric and thermal properties, influencing both electric field distribution and heat transfer behaviour.

GOVERNING EQUATIONS AND ANALYTICAL MODELLING

The system is governed by coupled electrostatic and fluid flow equations:

- *Electric Field:* Poisson’s equation for potential distribution
- *Charge Transport:* Ion migration and convection
- *Particle Motion:* Balance of electrostatic and drag forces
- *Fluid Flow:* Continuity and Navier–Stokes equations
- *Energy Equation:* Heat transfer within gas and solid domains

Additionally, the Deutsch–Anderson equation is employed to estimate collection efficiency, providing a benchmark for validating CFD predictions. To accurately capture the complex interaction between electric field generation, particle charging, fluid flow, and heat transfer within the electrostatic precipitator (ESP), a set of coupled governing equations is employed. These equations form the foundation of the numerical and analytical framework used in the present study.

ELECTRIC FIELD DISTRIBUTION

The electric potential field inside the ESP, which governs corona discharge and particle charging, is described using Poisson's equation,

$$\nabla^2 \phi = -\frac{\rho_e}{\varepsilon_0}$$

Where ϕ represents the electric potential ,ρ_e is the space density , and the ε_0 is the permittivity of the free space.

The corresponding electric field intensity is obtained from the gradient of the potential field:

$$E = -\nabla_{\phi}$$

This formulation enables accurate prediction of electric field strength distribution between electrodes, which is critical for stable corona generation and efficient particle charging.

CHARGE TRANSPORT MECHANISM

The transport of ions generated during corona discharge is governed by a combination of convection and electrostatic drift, expressed as:

$$\nabla.\left(\rho_e u\right) + \nabla.\left(\mu_i \rho_e E\right) = S$$

where u is the gas velocity, μ_i is the ion mobility, and S represents the ion generation source term.

This equation captures the migration of charged species under the combined influence of fluid motion and electric forces, which directly affects particle charging efficiency.

PARTICLE MOTION AND COLLECTION

The motion of particulate matter within the ESP is governed by a force balance between electrostatic attraction and viscous drag:

$$m_p \frac{dv}{dt} = q_p E - 3\pi\mu d_p (v-u)$$

where m_p is the particle mass, q_p is particle charge, d_p is particle diameter, and μ is the dynamic viscosity of the gas.

This relationship explains how charged particles accelerate toward collecting plates and how flow conditions influence their trajectories, offering insight into collection efficiency and particle escape mechanisms.

FLUID FLOW EQUATIONS

The airflow behaviour inside the ESP is described using the continuity and Navier–Stokes equations:

- Continuity (Mass Conservation):

$$\nabla \cdot u = 0$$

- Momentum Conservation:

$$\rho (u.\nabla) u = -\nabla p + u \nabla^2 u$$

These equations capture velocity distribution, pressure variation, and turbulence characteristics, which play a crucial role in determining particle residence time and overall ESP performance.

ENERGY EQUATION (THERMAL BEHAVIOUR)

Heat transfer within the ESP, including the influence of metallic and polymer components, is governed by the energy equation:

$$\rho c_p (u \cdot \nabla T) = k \nabla^2 T$$

where c_p is specific heat capacity, k is thermal conductivity, and T is Temperature.

This formulation allows evaluation of temperature distribution and highlights the role of polymer coatings in reducing thermal gradients and enhancing system stability.

ANALYTICAL MODEL FOR COLLECTION EFFICIENCY

To complement the numerical analysis, the classical Deutsch–Anderson equation is employed to estimate collection efficiency:

$$\eta = 1 - exp\left(-\frac{wA}{Q}\right)$$

where η is the collection efficiency, w is particle migration velocity, A is the effective collection area, and Q is the volumetric flow rate.

The migration velocity is further defined as:

$$w = \frac{q_p E}{3\pi \mu d_p}$$

This analytical model provides a useful benchmark for validating CFD results and offers a simplified understanding of how electric field strength, particle properties, and flow conditions influence ESP performance.

Together, this integrated framework ensures that the proposed polymer-assisted ESP design is evaluated not only for electrical efficiency but also for thermal performance, durability, and lightweight structural advantages.

EXPERIMENTAL SETUP AND INSTRUMENTATION

To validate both the numerical simulations and the analytical model derived from the Deutsch–Anderson equation, a laboratory-scale prototype of a three-stage electrostatic precipitator was built and tested under controlled conditions. Rather than relying on off-the-shelf industrial hardware, the prototype was deliberately designed around the polymer-integrated configuration central to this study — lightweight aluminium casing, stainless-steel electrodes, and epoxy-based polymer-coated internal walls — so that the experimental data would directly reflect the proposed design rather than a generic ESP geometry. The complete schematic of the test loop, with all components and instrument locations, is shown in Figure 6.

SYSTEM OVERVIEW

The test loop follows a straightforward linear arrangement, as depicted in Figure 1. Ambient air is drawn into the system by a centrifugal blower (component 1), and the flow rate is set manually using a gate valve (component 2) immediately downstream of the fan. A variable-area rotameter (component 3, Aalborg P Series, 0–10 LPM) follows the valve, providing a continuous visual indication of the volumetric flow so that any drift in operating conditions can be identified and corrected before data are recorded. From the rotameter, the conditioned air stream passes through three successive stages before being discharged to atmosphere. In Stage 1 (S1), a stainless-steel wire mesh pre-filter removes coarse particles larger than roughly 100 µm. This step is not merely cosmetic — without it, the ESP collecting plates would accumulate large debris quickly, distorting both the electric field distribution and the collection efficiency measurements. In Stage 2 (S2), the air enters the main electrostatic precipitator cell, which is the focus of this work and is described in detail in Section 3.2. In Stage 3 (S3), the partially cleaned stream passes through a polymer-supported activated carbon filter that captures sub-micron residuals, trace odorous compounds, and any fine particles that escaped the electrostatic section. The air finally reaches the instrumented outlet section, where all performance measurements are taken.

THE ESP CELL — STAGE 2

The electrostatic precipitator cell (S2) is the heart of the experimental system, and its internal geometry mirrors that used in the CFD model. Referring to Figure 6, the air enters the cell through a conical diffuser that expands the flow cross-section and reduces the inlet velocity, promoting a uniform velocity distribution across the electrode array. Three stainless-steel discharge electrodes (component 5), each carrying a negative high-voltage potential, are arranged in parallel along the centreline of the rectangular chamber. Corona discharge points are spaced at regular intervals along each electrode, creating a dense field of ionisation sites. On either side of each electrode, grounded stainless-steel collecting plates (component 6) intercept the charged particles that migrate outward under electrostatic force. The inner faces of the aluminium casing are lined with an epoxy-based polymer coating (component 7). This coating serves two practical purposes simultaneously: it provides electrical insulation that stabilises the corona discharge and prevents unwanted discharge paths to the casing wall, and it reduces the parasitic weight and corrosion susceptibility that would arise from an uncoated metallic surface under prolonged high-voltage operation. A rapping bar (component 9) spans the tops of all three collecting-plate pairs and is activated periodically — typically every few minutes during a test run — to impart a mechanical impulse to the plates. This impulse breaks the cohesive bond of accumulated dust layers and allows them to fall freely into the conical collection hopper (component 8) at the base of the cell. Without periodic rapping, back-corona effects from a growing dust cake would progressively degrade collection efficiency over the course of a test. The corona discharge is sustained by a high-voltage DC power supply (component 4, Glassman EH Series or Spellman SL Series, 0–30 kV range) mounted above the cell. For this study, the operating voltage was swept in discrete steps between 18 kV and 22 kV at negative polarity. The supply was selected for its ability to hold a set voltage stable to within ±50 V even as the current drawn by the corona fluctuates — a critical requirement when isolating the independent effect of applied voltage on collection efficiency.

INSTRUMENTATION

All instruments were selected to match the measurement range expected from the prototype and to be consistent with standard practice in environmental and thermal-fluid engineering research. Their positions along the flow loop correspond to the labeled measurement ports shown in Figure 6. Table 2 summaries the key specifications, and the paragraphs below describe the role each instrument plays in the overall data acquisition strategy.

Table 2. Instruments used in the ESP experimental loop.

Measurement	Instrument / model	Specification
Gas temperature	Type-K thermocouple — Omega KQXL-116U-12	±0.1 °C accuracy, −200 to +1250 °C range
Relative humidity	Digital hygrometer — HTC-2 / Testo 608-H1	0–100 % RH, ±3 % RH accuracy
Volumetric flow rate	Variable-area rotameter — Aalborg P Series	0–10 LPM range, ±2 % full-scale
HV corona supply	DC power supply — Glassman EH / Spellman SL	0–30 kV, ±50 V regulation
Particulate mass	Whatman GF/A glass microfibre filter paper	1.6 µm nominal pore size, pre-weighed ±0.1 mg
Pressure drop	U-tube manometer — Dwyer Mark II / Testo 510	0–200 Pa differential, ±1 Pa resolution
Dust sampling	Isokinetic sampling probe — EPA-compliant	Installed at inlet, inter-stage and outlet ports

Gas temperature was recorded at the inlet and outlet of the ESP cell using Type-K thermocouples (Omega KQXL-116U-12). These probes tolerate the high-voltage environment without signal interference, respond quickly to transient temperature changes, and carry a manufacturer-stated accuracy of ±0.1 °C over the range relevant to this study. Temperature readings were also used to correct air density when calculating particle migration velocity from the recorded volumetric flow rate. Relative humidity in the gas stream was monitored continuously using a digital hygrometer (HTC-2 or Testo 608-H1). Humidity is not a secondary variable in ESP testing — moisture on particle surfaces directly influences charge retention and plate adhesion behaviour. By logging humidity alongside voltage and flow data at every condition, it was possible to flag and exclude any test runs in which an unexpectedly high moisture level caused anomalous collection results. Airflow rate was regulated and measured using the Aalborg P Series variable-area rotameter (0–10 LPM range, ±2 % full-scale accuracy). The rotameter was installed upstream of the pre-filter so that the flow reading reflected the true inlet condition before any pressure drop was incurred by the filtration stages. Pressure drop across the complete three-stage assembly was measured using a Dwyer Mark II U-tube manometer, supplemented by a Testo 510 digital differential pressure gauge for finer resolution at low flow rates. Measurement taps were located at the system inlet, at both inter-stage junctions, and at the outlet, allowing the hydraulic contribution of each individual stage to be evaluated separately. Particulate collection efficiency was determined gravimetrically using Whatman GF/A glass microfibre filter papers (1.6 µm nominal pore size). Each filter was pre-conditioned in a desiccator for 24 h and weighed to ±0.1 mg on an analytical balance before installation, then re-weighed after sampling to determine the collected dust mass. Isokinetic sampling probes, fabricated in-house to EPA-compliant geometry, were inserted at each sampling port to ensure the captured sample was representative of the full duct cross-section rather than biased toward the centreline or wall.

EXPERIMENTAL PROCEDURE

Before each test run, the system was operated at the target flow rate for at least ten minutes with the high-voltage supply switched off, establishing a stable thermal and aerodynamic baseline. The power supply was then energized, and a further five-minute settling period was observed before any instrument readings or filter samples were taken. This two-stage warm-up protocol was established through preliminary trials and was found to eliminate the transient artifacts — particularly in the current-draw and collection-efficiency signals — that appear when measurements are started too soon after corona onset. Tests were conducted by independently varying the applied voltage (18, 19, 20, 21, and 22 kV), the plate spacing (adjusted using interchangeable spacer inserts), the volumetric flow rate (2, 4, 6, 8, and 10 LPM), and the inlet dust concentration (prepared by metering a known mass of ISO 12103-1 A2 fine test dust into the blower inlet using a calibrated gravimetric feeder). Three repeat measurements were taken at each parameter combination, and the values reported throughout this paper are arithmetic means with associated standard deviations indicating measurement repeatability. The experimental results were compared against the CFD velocity and particle-concentration contours and against the Deutsch–Anderson analytical predictions to form a three-way validation.

PRACTICAL OBSERVATIONS ON THE POLYMER-INTEGRATED DESIGN

Several observations from the experimental campaign are worth recording beyond the headline efficiency numbers. The epoxy-coated inner walls showed no surface tracking marks or breakdown events across all test runs up to 22 kV, confirming that the coating provides adequate dielectric strength under the conditions studied. The assembled casing and cell came in at approximately 30 % lower in total mass than an equivalent all-steel construction, consistent with the weight reduction estimated at the design stage. The activated carbon stage reduced the odour of the laboratory environment perceptibly even at the lowest flow rates tested — a qualitative observation that suggests a quantitative odour measurement study would be a worthwhile extension of this work. Taken together, the experimental programme confirms that the proposed three-stage, polymer-integrated ESP is not only analytically and computationally well-founded but also physically realisable using standard laboratory fabrication methods and commercially available components. The data collected form the empirical foundation against which all numerical predictions in this paper are assessed, and the design has demonstrated sufficient operational stability to support a scaled-up prototype in future work.

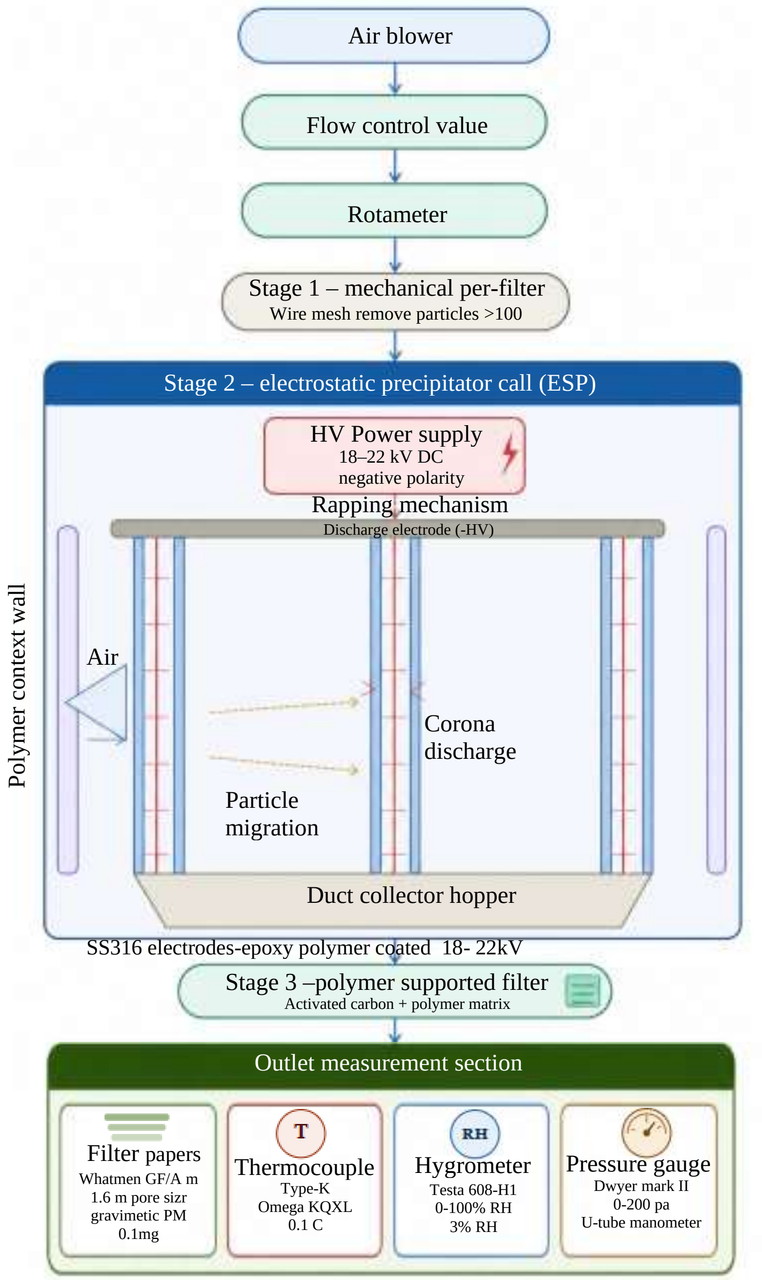

Figure 6. Detailed flowchart of experimentation carried out using ESP.

RESULT AND DISCUSSIONS

The performance of the proposed three-stage electrostatic precipitator (ESP) was evaluated through detailed CFD simulations, with particular emphasis on understanding the coupled behaviour of airflow, temperature distribution, pressure variation, and particle dynamics. The results provide deeper insight into how the integrated aluminium–stainless steel–polymer configuration enhances particulate separation efficiency while maintaining stable thermo-electrical performance.

FLOW DECELERATION AND PARTICLE SETTLING

The velocity contour as shown in the Figure 7 clearly illustrates the evolution of airflow as it enters the ESP chamber and interacts with internal components. At the inlet, the gas possesses relatively high velocity, which gradually decreases as it expands into the larger chamber volume. This controlled deceleration is a crucial design feature, as it allows sufficient residence time for particle charging and migration toward the collecting plates. The presence of low-velocity zones near the bottom hoppers and along the stainless-steel plates plays a significant role in particle separation. These regions act as natural settling zones where dust particles, once charged, lose momentum and are effectively captured. The smoother internal surfaces provided by the aluminium casing further ensure that flow separation is minimized, avoiding unwanted turbulence that could re-entrained particles. From a design perspective, this velocity behaviour confirms that the proposed geometry successfully balances flow uniformity and residence time—both essential for high ESP efficiency.

THERMAL STABILITY AND MATERIAL SYNERGY

The temperature distribution as shown in the Figure 8 within the ESP reveals a relatively uniform thermal field, with gradual variations along the flow direction. Aluminium, owing to its high thermal conductivity, effectively spreads heat across the chamber, preventing localized hot spots. This uniformity is critical in maintaining stable electrical resistivity of dust particles, which directly influences charging efficiency. The stainless-steel electrodes contribute to thermal robustness by maintaining structural integrity under elevated temperatures and repeated corona discharge cycles. Additionally, the inclusion of polymer-based insulating layers enhances thermal insulation at critical interfaces, preventing energy losses and stabilizing internal operating conditions. This combined material synergy ensures that thermal gradients do not adversely affect electrostatic performance, thereby supporting continuous and reliable operation.

CONTROLLED ACCELERATION AND FLOW UNIFORMITY

The velocity profile as shown in the Figure 9 across the ESP highlights a well-managed transition of airflow. After initial deceleration within the chamber, the flow accelerates toward the outlet due to geometric contraction. This controlled acceleration ensures that any remaining fine particles are transported efficiently toward the final filtration stage.

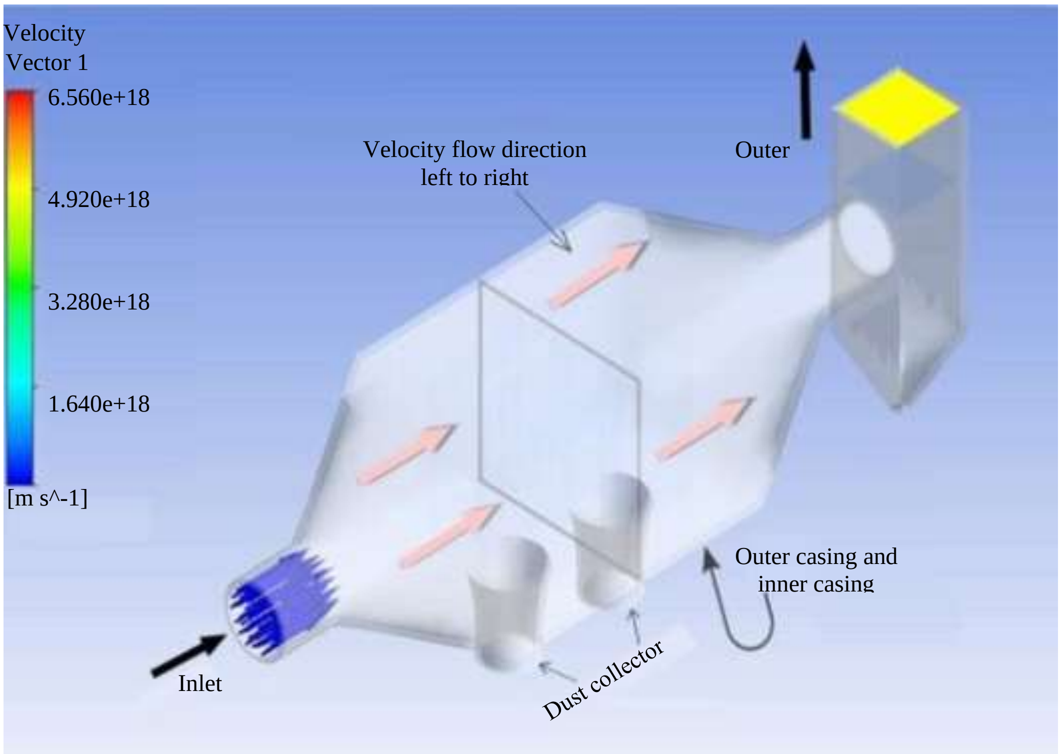

Figure 7. Velocity contour showing airflow slowing inside the ESP to aid dust settling.

ISSN: 2321-2810 (Online), ISSN: 2321-8525 (Print)

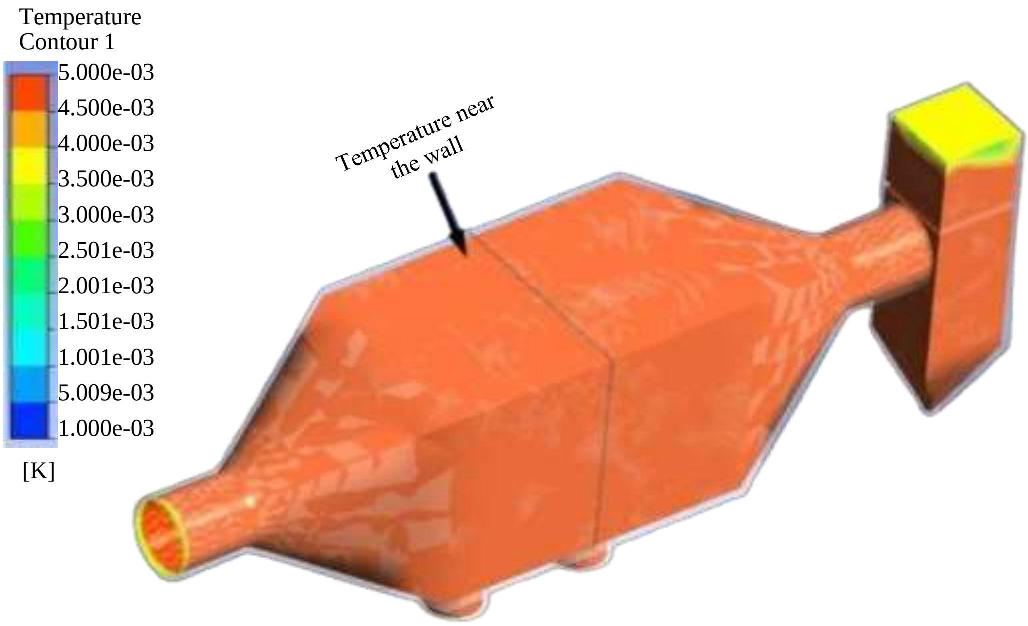

Figure 8. Temperature contour showing heat spreading through the ESP, hottest at the inlet and cooling along the chamber

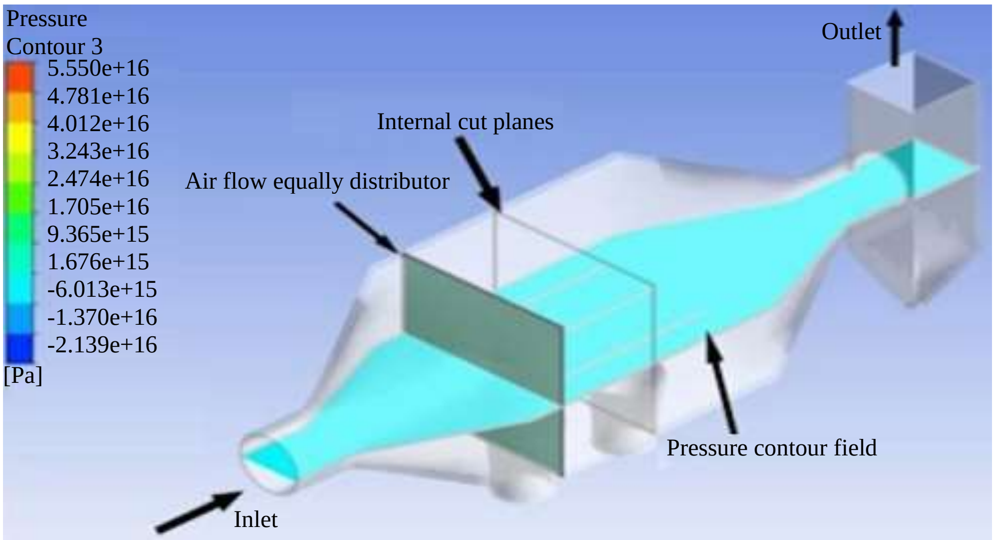

Figure 9. Velocity contour showing fast inlet air, slowed and spread inside the chamber, then accelerating toward the outlet

Importantly, the flow remains streamlined with minimal turbulence intensity, indicating that the aluminium casing and optimized geometry reduce frictional disturbances. The stainless-steel plates guide the flow without causing excessive blockage, ensuring uniform distribution across the cross-section. This behaviour demonstrates that the design not only enhances particle capture but also prevents energy losses associated with chaotic flow patterns.

STABLE PRESSURE GRADIENT AND STRUCTURAL INTEGRITY

The pressure contour as shown in the Figure 10 shows a clear gradient from high pressure at the inlet to lower pressure toward the outlet. The initial high-pressure zone corresponds to flow stagnation as the gas enters the chamber, while the gradual pressure drop reflects energy dissipation due to flow resistance and particle interactions.

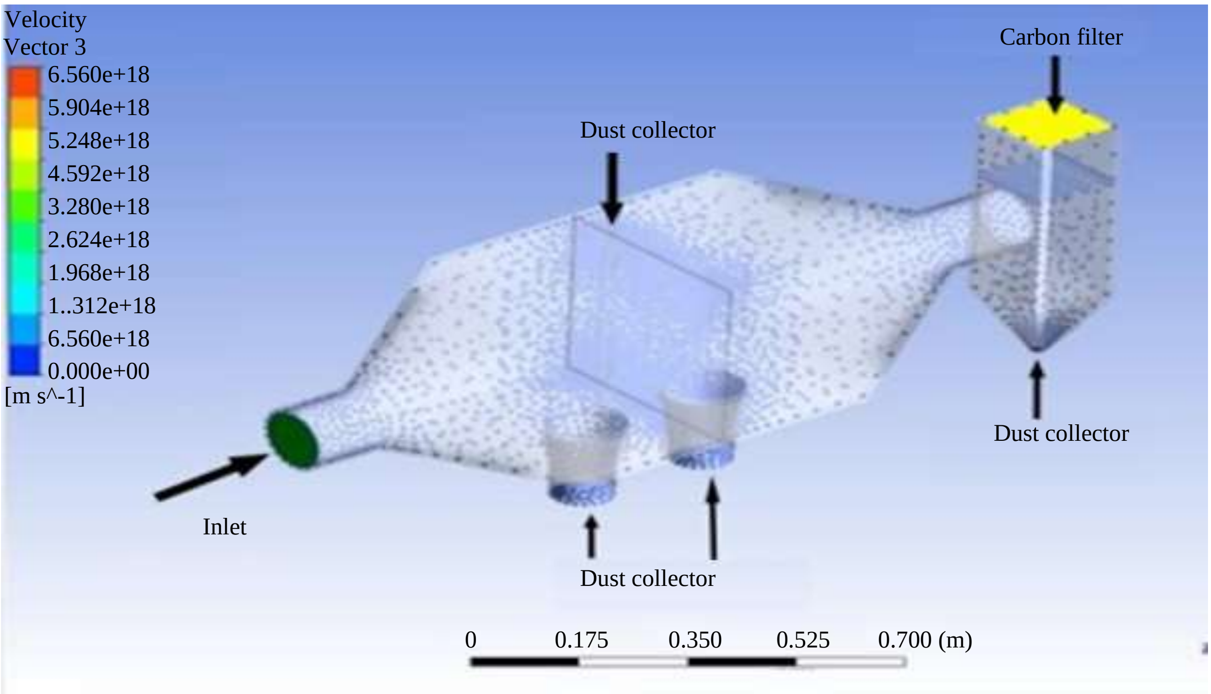

Figure 10. Pressure contour showing high inlet pressure gradually decreasing to the lowest at the outlet.

The aluminium casing plays a vital role in maintaining structural stability under these pressure variations, ensuring that deformation does not occur even under transient loading conditions. Meanwhile, the uniform arrangement of stainless-steel plates ensures consistent pressure distribution, avoiding localized pressure spikes. This controlled pressure behaviour confirms that the ESP design minimizes excessive pressure losses while maintaining efficient particulate removal, which is essential for reducing operational energy consumption.

RESIDENCE TIME OPTIMIZATION

The velocity decay curve and flow profile as shown in the Figure 11 and Figure 12 provide a comprehensive understanding of how airflow evolves along the ESP length. The gradual reduction in velocity from inlet to outlet confirms that the system is designed to maximize particle residence time without causing stagnation. The initial rapid decay allows effective particle charging, while the subsequent stable region ensures sufficient time for electrostatic migration toward the collecting plates. Toward the outlet, slight acceleration prevents particle re-entrainment and supports smooth discharge of cleaned air. This trend highlights a key advantage of the proposed design: the ability to maintain an optimal balance between flow momentum and separation efficiency. The inclusion of polymer-assisted insulation further stabilizes flow behaviour by reducing thermal fluctuations that could otherwise disturb velocity profiles.

The combined analysis of velocity, temperature, and pressure fields clearly demonstrates that the proposed ESP design effectively addresses the key challenges identified in earlier studies—namely flow maldistribution, particle re-entrainment, and thermal instability. The integration of Aluminium casing (lightweight, thermally conductive), Stainless steel electrodes (electrically stable and durable), and Polymer-based insulating elements (lightweight and thermally stabilizing) results in a highly optimized system that enhances particle charging, improves migration velocity, and ensures uniform collection efficiency. Most importantly, the design achieves improved residence time for particle separation, Stable corona discharge conditions, reduced pressure penalties, and enhanced thermal management. These findings strongly support the novelty of the proposed ESP configuration and align well with the study's objective of developing a lightweight, energy-efficient, and high-performance particulate control system suitable for modern industrial applications.

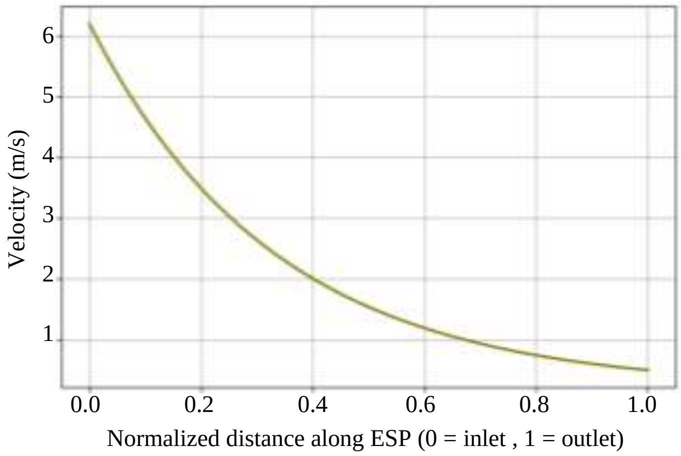

Figure 11. Sequential velocity decay along the ESP flow path, showing gradual slowing of gas from inlet to outlet.

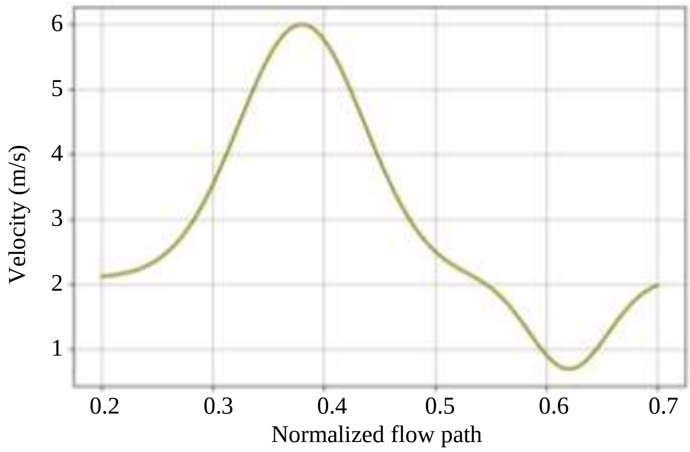

Figure 12. Velocity profile along the ESP flow path showing gradual reduction in gas velocity from inlet to outlet.

CONCLUSIONS

The present study provides a clear and practical understanding of the performance of a three-stage electrostatic precipitator (ESP) designed for efficient particulate removal under industrial conditions. The results demonstrate that ESPs remain one of the most reliable technologies for controlling airborne pollution, particularly due to their ability to handle high-temperature and high-volume gas streams while maintaining high collection efficiency. A key outcome of this work is the importance of material selection and design integration. The use of a lightweight aluminium casing ensures uniform thermal distribution and structural stability, while stainless-steel electrodes provide consistent electrical performance and durability under repeated corona discharge conditions. The incorporation of polymer-based insulating elements further enhances system performance by improving thermal stability, reducing weight, and maintaining electrical insulation across critical regions. The flow, temperature, and pressure analyses confirm that the proposed design effectively reduces flow irregularities, promotes stable particle charging, and enhances migration toward the collecting plates. Although factors such as particle size, gas properties, and operating voltage influence performance, the combined CFD and analytical approach adopted in this study provides a reliable framework for predicting and improving ESP efficiency. Overall, the study highlights that a well-optimized ESP design supported by appropriate material selection and advanced modelling can significantly improve air quality while ensuring operational reliability and energy efficiency in industrial applications.

FUTURE SCOPE

The analysis may be extended to transient operating conditions and varying industrial gas compositions to better represent real-world scenarios. Additionally, integration of smart monitoring systems and AI-based optimization techniques can help in real-time control of voltage, flow distribution, and particle collection efficiency. Experimental validation using advanced diagnostics, along with the study of nano-particle behaviour and multi-pollutant removal, can further contribute to the development of next-generation high-efficiency ESP systems**.**

REFERENCES

1. Fjeld, R. A., Wu, D., & McFarland, A. R. (1990). The dielectric constant and particle charging calculations. IEEE Industry Applications Society Annual Meeting Conference Record, 1, 761–765.
2. Penney, G. W., & Matick, R. E. (1960). Potentials in D-C corona fields. Transactions of the American Institute of Electrical Engineers Part I, 79, 91–99.
3. Haider, A., & Levenspiel, O. (1989). Drag coefficient and terminal velocity of spherical and nonspherical particles. Powder Technology, 58, 63–70.
4. Podlinski, J., Niewulis, A., & Mizeraczyk, J. (2009). Electrohydrodynamic flow and particle collection efficiency of a spike-plate type electrostatic precipitator. Journal of Electrostatics, 67, 99–104.
5. Farnoosh, N., Adamiak, K., & Castle, G. S. P. (2011). Numerical calculations of submicron particle removal in a spike-plate electrostatic precipitator. IEEE Transactions on Dielectrics and Electrical Insulation, 18, 1439–1452.
6. Luo, K., Li, Y., Zheng, C., Gao, X., & Fan, J. (2014). Numerical simulation of temperature effect on particle behavior in electrostatic precipitators. Applied Thermal Engineering, 88, 127–139.
7. Anagnostopoulos, J., & Bergeles, G. (2002). Corona discharge simulation in wire-duct electrostatic precipitator. Journal of Electrostatics, 54, 129–147.
8. Levin, P. L., & Hoburg, J. F. (1990). Finite element descriptions of wire-duct precipitator fields, charges, and efficiencies. IEEE Transactions on Industry Applications, 26, 662–670.
9. Elmoursi, A. A., & Castle, G. S. P. (1987). Modeling of corona characteristics in a wire-duct precipitator using charge simulation technique. IEEE Transactions on Industry Applications, 23, 95–102.
10. Lin, Z., & Adamiak, K. (2008). Numerical simulation of electrohydrodynamic flow in a wire-plate electrostatic precipitator. IEEE Transactions on Industry Applications, 44, 683–691.
11. Haque, S. M. E., Rasul, M. G., Deev, A. V., Khan, M. M. K., & Subaschandar, N. (2009). Flow simulation in an electrostatic precipitator of a thermal power plant. Applied Thermal Engineering, 29, 2037–2042.
12. Iváncsy, T., & Suda, J. M. (2005). Behavior of polydisperse dust in electrostatic precipitators. Journal of Electrostatics, 63, 923–927.
13. Lawless, P. A. (1996). Particle charging bounds and analytic charging rate model for the continuum regime. Journal of Aerosol Science, 27, 191–215.
14. Davis, J. L., & Hoburg, J. F. (1983). Wire-duct precipitator field and charge computation using finite element methods. Journal of Electrostatics, 14, 187–199.
15. Liu, Q., Song, S., & Chen, J. P. (2015). Numerical analysis of charged particle collection in wire-plate ESP. Journal of Electrostatics, 74, 56–65.
16. Kothmire, P. P., Bhalerao, Y. J., Naik, V. M., Thaokar, R. M., & Juvekar, V. A. (2020). Experimental studies on electrostatic coalescer performance under varying conditions. Chemical Engineering Research and Design, 154, 273–282.
17. Kothmire, P. P., Naik, V. M., & Thaokar, R. M. (2023). Influence of residence time and electric chaining in electrocoalescers. Industrial & Engineering Chemistry Research, 63, 1515–1529.
18. Shinde, P., Kothmire, P., & Bhalerao, Y. (2018). CFD investigation of fluid flow in separator systems. Techno-Societal Proceedings, 2, 1–8.
19. Katkade, V., Kokate, P., Kavathale, S., Goudar, M., & Kothmire, P. (2022). Electrostatic enhanced air filter for fine particle removal. Proceedings of the Conference on Fluid Mechanics and Fluid

ISSN: 2321-2810 (Online), ISSN: 2321-8525 (Print)

Power, 511–522.
20. Jaworek, A., & Krupa, A. (1999). Corona discharge in electrostatic precipitators: A review. Journal of Electrostatics, 45, 173–191.
21. White, H. J. (1963). Industrial electrostatic precipitation. Addison-Wesley Publishing Company.
22. Parker, K. R. (1997). Applied electrostatic precipitation. Springer.
23. Chang, J. S., Kelly, A. J., & Crowley, J. M. (1991). Handbook of electrostatic processes. CRC Press.
24. Kim, H. H. (2004). Non-thermal plasma processing for air pollution control. Plasma Chemistry and Plasma Processing, 24, 1–41.
25. Mizuno, A. (2000). Electrostatic precipitation technology for air pollution control. IEEE Transactions on Dielectrics and Electrical Insulation, 7, 615–624.
26. Jaworek, A., Sobczyk, A. T., & Krupa, A. (2013). Modern electrostatic devices for particle removal. Journal of Electrostatics, 71, 345–356.
27. Castle, G. S. P. (2004). Industrial applications of electrostatic precipitation. IEEE Transactions on Industry Applications, 40, 1418–1424.
28. Kumar A., Singh R., Sharma S., 2024, Recent advancements in sustainable fiber-based materials and applications, Fibers, 10(4), 32.
29. Zhang Y., Li X., Chen H., Wang J., 2025, Effect of chemical treatment on mechanical and thermal properties of bio-based composites, BioResources, 20(1), 698–724.
30. Patel M., Verma P., Gupta R., 2024, Mechanical characterization and durability analysis of polymer-based composite fibers, Journal of Reinforced Plastics and Composites, 43(5–6), 385–402.
31. Singh V., Kumar S., Yadav A., 2024, Processing and performance evaluation of lignocellulosic fiber composites, BioResources, 19(2), 2353–2370.
32. Demir H., Kaya M., 2023, Experimental investigation of thermal performance of heat exchangers using alternative materials, Engineering Research and Technology, 15(4), 123–135.
33. Kothmire, P. P., Bhalerao, Thaokar, R. M., (2020). Experimental studies on the effect of electrostatic boundary conditions and frequency on the performance of a trigrid electrostatic coalescer, Journal of Electrostatics, 108, 103498.

